GEO387H Physical Climatology
Fall 2007

Literature Review:

Simulating land-surface processes in transition zones with enhanced versions of Noah LSM

Enrique Rosero

Department of Geological Sciences
Jackson School of Geosciences

THE UNIVERSITY OF TEXAS AT AUSTIN

Outline:

Motivation:

The importance of turbulent fluxes in transition zones for summer time convection initiation

Simulating land memory mechanisms with the Noah Land Surface Model:

Role of vegetation: Stomatal control on evaporation

Role of soil moisture: High resolution initialization

Parameterization issues and inverse modeling

Summary

Relevance of transition zones

Hotspots for land-atmosphere coupling: anomalies in surface states propagate to atmosphere and influence precipitation

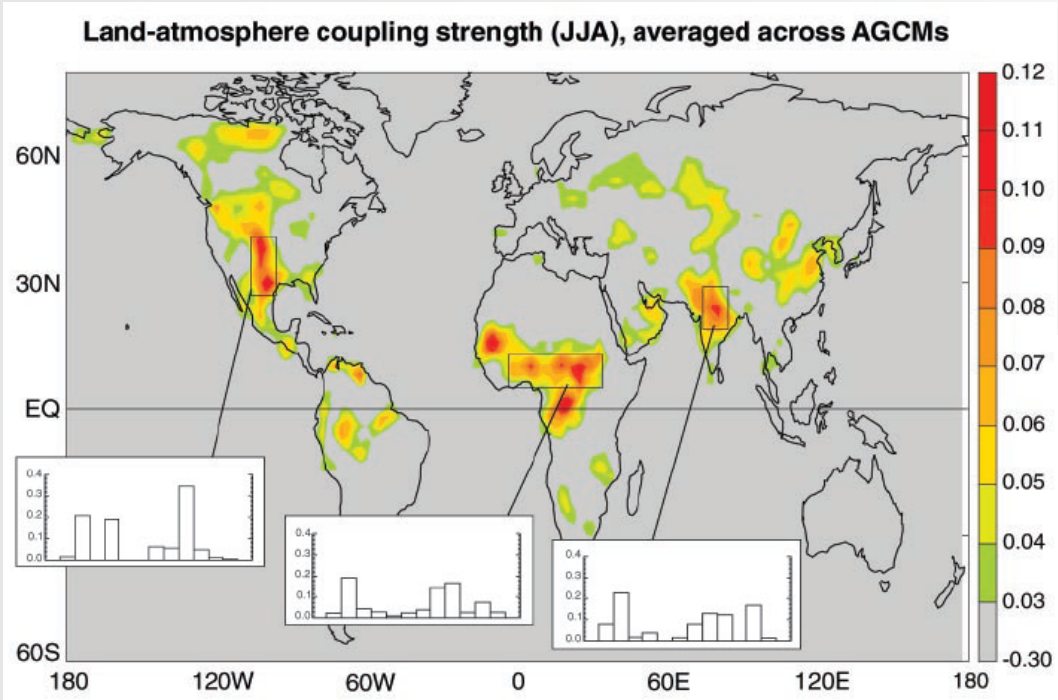

Fig. 1. The land-atmosphere coupling strength diagnostic for boreal summer (the Ω difference, dimensionless, describing the impact of soil moisture on precipitation), averaged across the 12 models participating in GLACE. (**Insets**) Areally averaged coupling strengths for the 12 individual models over the outlined, representative hotspot regions. No signal appears in southern South America or at the southern tip of Africa.

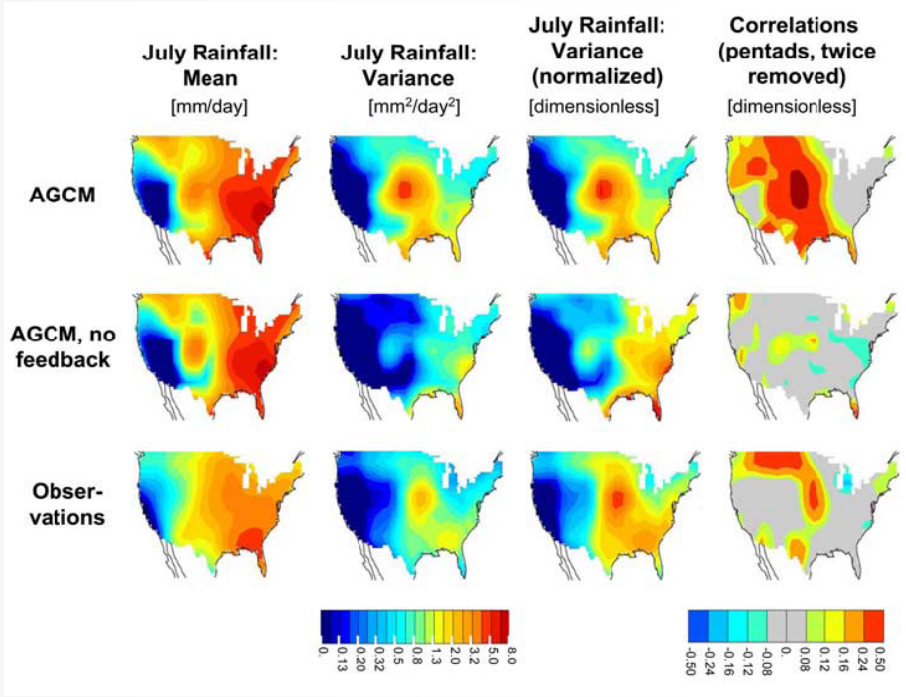

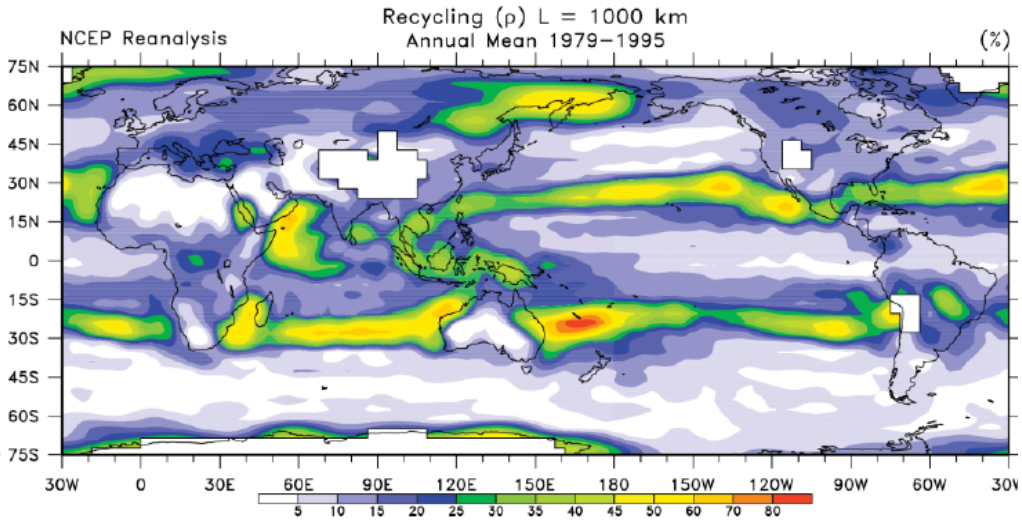

Fig. 2. Estimate of the annual mean recycling ratio of the percentage precipitation coming from evaporation within a length scale of 1000 km (adapted from Trenberth 1999b).

JACKSON SCHOOL OF GEOSCIENCES

Koster et al. 2004; Koster et al. 2003; Trenberth et al. 2003

Summertime convection initiation

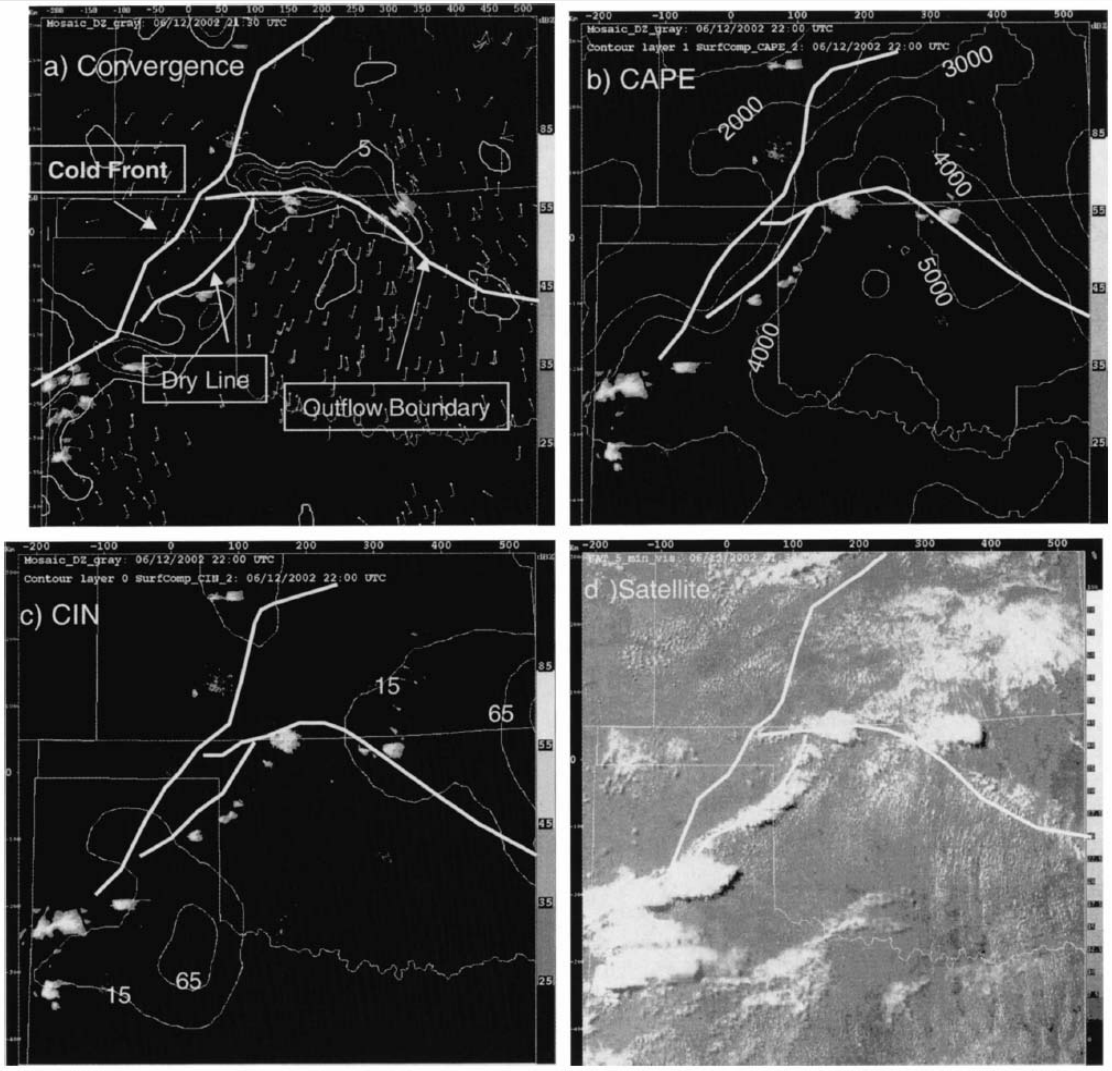

FIG. 8. At 2140 UTC 12 June, boundaries (solid heavy white lines) overlaid on (a) radar reflectivity (grayscale shades on right in dBZ) and convergence (first contour 5×10^{-4} s^{-1} with contour interval of 5×10^{-4} s^{-1}), (b) radar reflectivity and CAPE (contour interval of 1000 J kg^{-1}), (c) radar reflectivity and CIN (first contour 15 J kg^{-1} with contour interval of 50 J kg^{-1}), and (d) visible satellite.

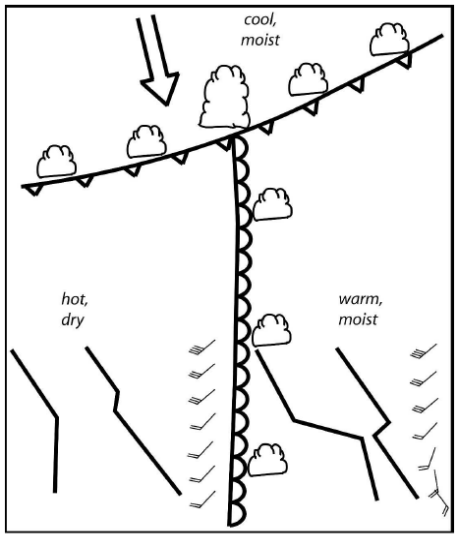

FIG. 5. Conceptual model of cold front–dryline intersection. The baroclinic boundary is indicated by a barbed line while the dryline is depicted with half circles. Large arrow depicts general flow field. Schematic clouds show the relative size and frequency along the dryline and cold front in contrast to deeper convective development at the triple point. As presented in Weiss and Bluestein (2002), typical soundings on either side of the dryline are shown.

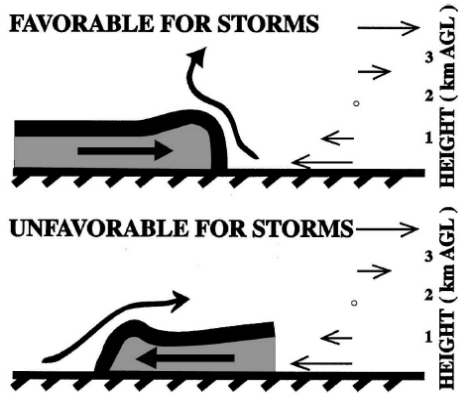

FIG. 3. Schematic illustration of dynamic conditions (top) favorable and (bottom) unfavorable for CI derived from observations in a relatively low shear environment. The wind vectors on the right represent the environmental wind profile, which is the same for both cases. The dark shading represents a density current, or boundary. The curved arrow ahead of the density current represents the updraft tilt. (From Wilson et al. 1998.)

Weckwert and Parsons 2006;

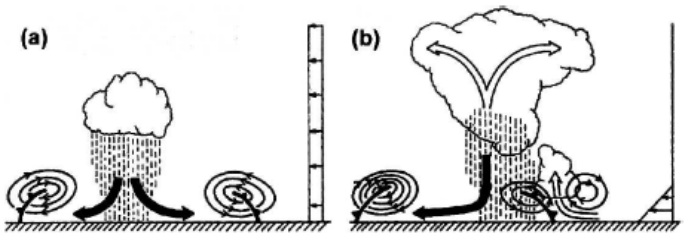

FIG. 2. Conceptual model of importance of low-level shear in the evolution of convection. (a) Without low-level shear, the cold-pool circulation inhibits deep vertical lifting and inhibits new convection. (b) With low-level shear countering the cold-pool circulation, new cells can be triggered. (From Rotunno et al. 1988.)

Wilson and Roberts 2006

Afternoon, high intensity showers are driven by convergent boundaries (triple point), drylines, and bores. In capped moist boundary layers, lifting is sensitive to low level wind shear.

Model biases in precipitation simulation

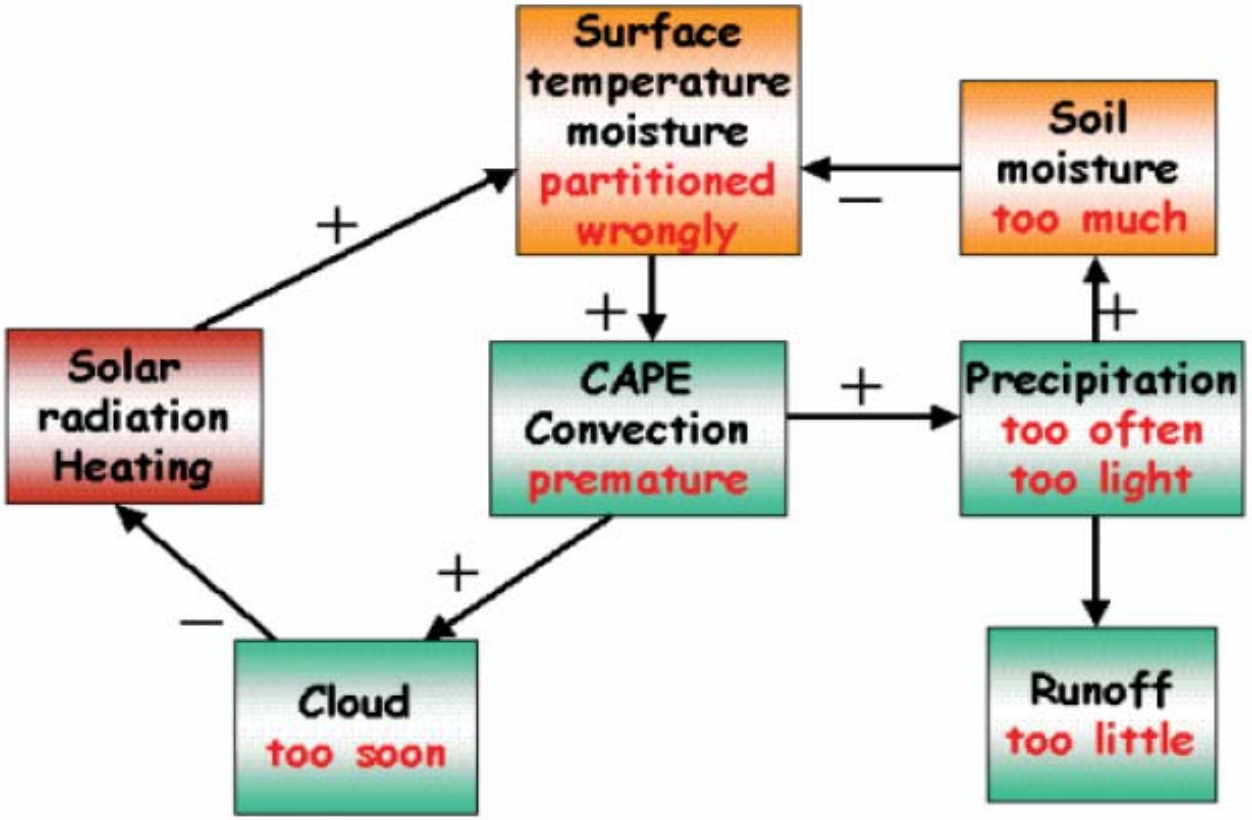

FIG. 5. Key feedback mechanisms involved in the diurnal cycle are given along with the model biases (in red). Trenberth et al. 2003

Premature initiation of convection and drizzling are known shortcomings of GCMs.

Model biases are related to land surface states and fluxes.

Accurate representation is key to simulate timing, duration and intensity of precipitation.

IHOP_2002: Collocated, multi-sensor observations

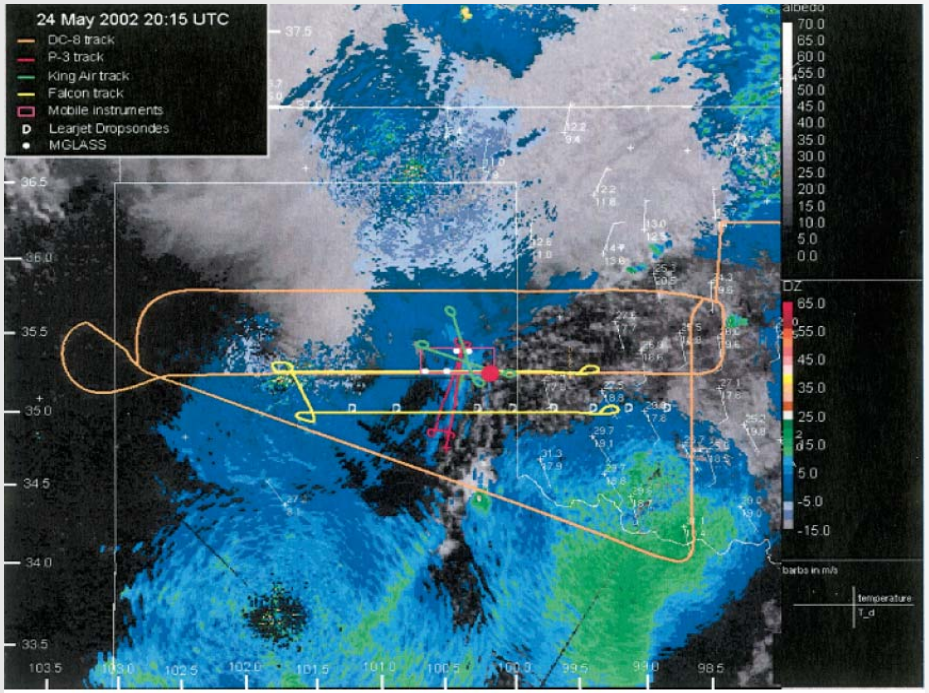

FIG. 7. Visible satellite and radar composite image on 2015 UTC 24 May 2002 prior to CI. Shown are the flight tracks of the various aircraft, the locations of the mobile ground-based systems, and the available surface station data, plotted with temperature (°C) on top, dewpoint temperature (°C) on bottom, and wind barbs with a full barb of 5 m s^{-1}. Shamrock, TX, is at the red circle.

Western Track Site 1: Bare Ground (Plowed)

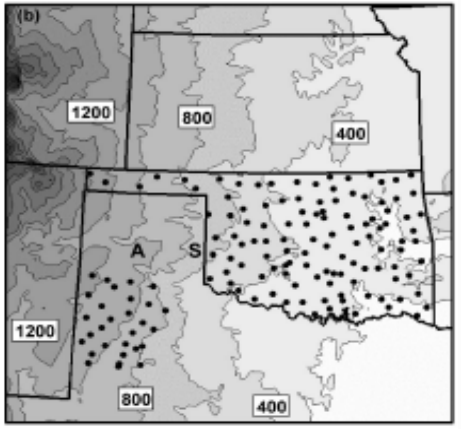

Central Track Site 5: Winter Wheat

Eastern Track Site 9: Grassland

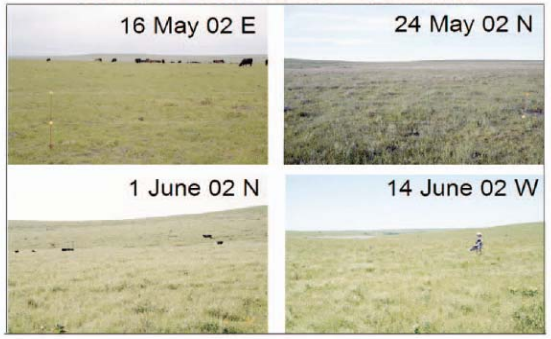

FIG. 3. Seasonal change of surface land use characteristics at three selected HOP_2002 sites. (top) Site 1 (bare ground, Western Track); (middle 4) site 5 winter wheat, Central track); (bottom 4) site 9 (grassland, Eastern Track).

Weckwerth et al. 2004; LeMone et al. 2007

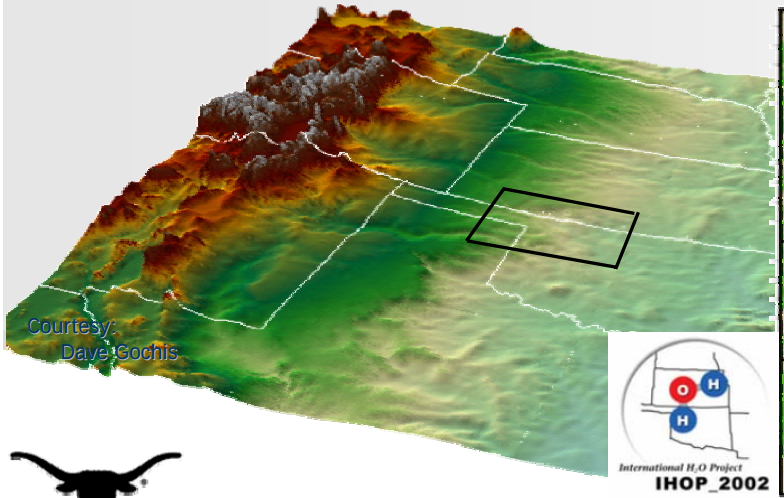

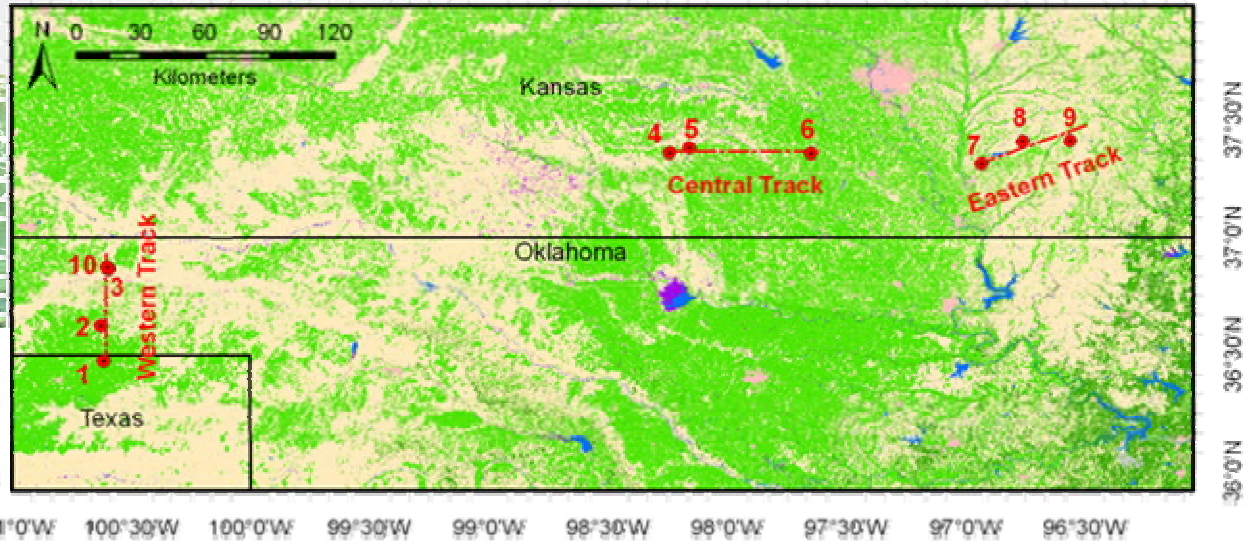

NCAR

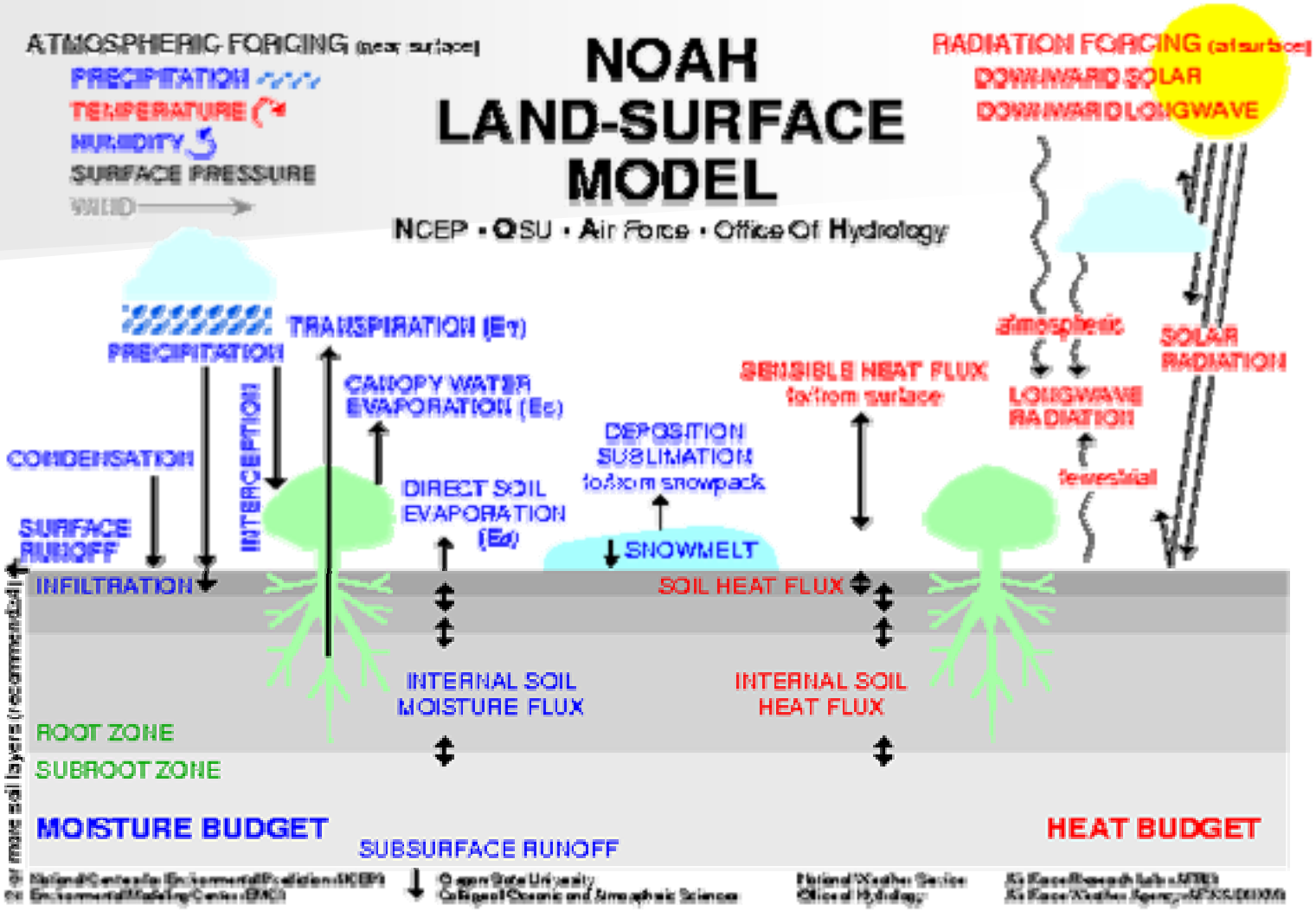

Ek et al. 2003; Mitchell et al. 2004

Land memory: the role of vegetation

Stomatal response to environmental variations control partition of net radiation and regulate soil moisture in the root zone. Jarvis parameterizes stress factors, while for Ball-Berry, considers transpiration as the cost of photosynthesis. Ball-Berry better represents observed values of canopy resistance.

$$g_s = g_n \, f_D(D) \, f_T(T) \, f_S(S) \, f_W(\theta) \quad (\mathrm{m\ s^{-1}})$$

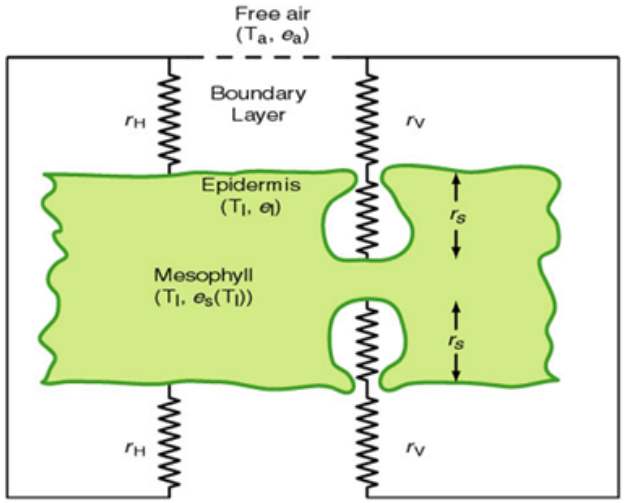

$$g_s = m\left(A_n / C_s\right) P_l F_e + g_{\min}$$

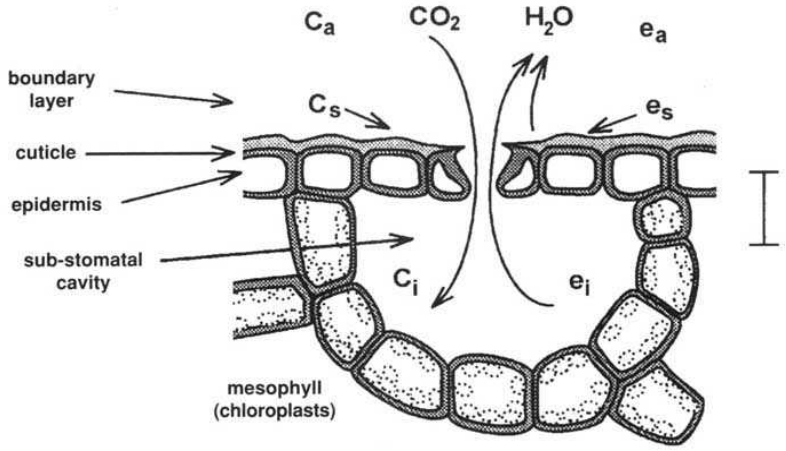

Shuttleworth 2007; Jarvis 1976; Ball and Berry 1987; Niyogi and Raman 199

Coupled simulations with GEM

Noah-WRF is enhanced with photosyntesis-based ET. Canopy resistance is 500% larger than Jarvis', transpiration rate is reduced by 60% and soil moisture is increased by 10%.

Holt et al. 2006

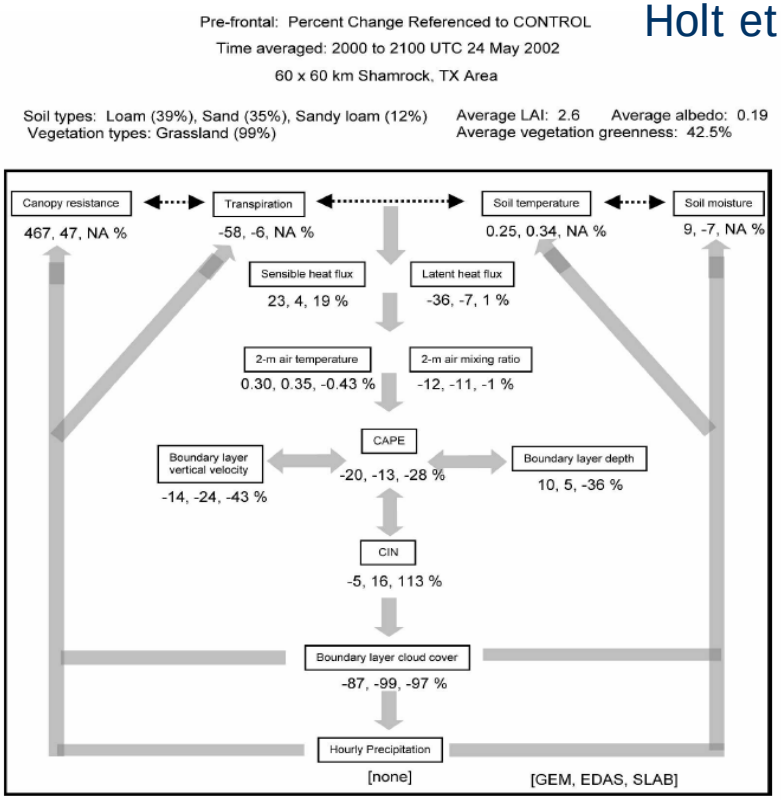

FIG. 17. Percent change of quantities for simulations GEM, EDAS, and SLAB relative to CONTROL values averaged from 2000 to 2100 UTC 24 May 2002 over the 60 km × 60 km Shamrock, TX, subset region (given by box S in Fig. 8a). Positive percent changes indicate an increase relative to the CONTROL values. This time is considered prefrontal, with no precipitation for any simulation from 2000 to 2100 UTC.

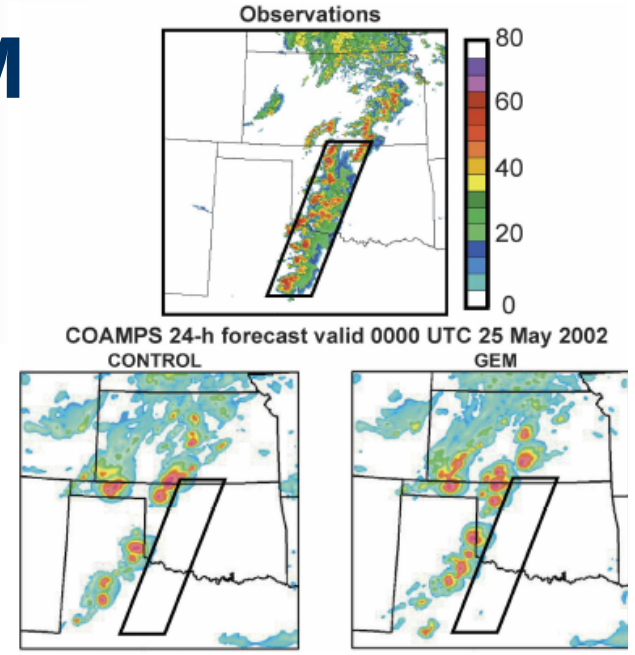

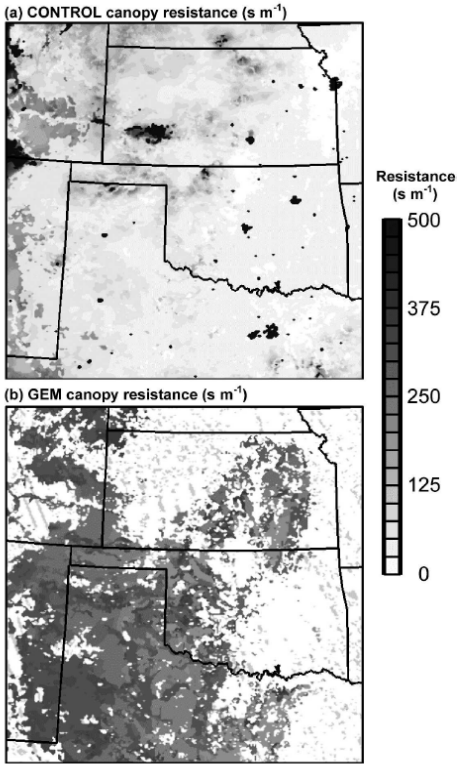

FIG. 14. The 21-h forecast valid 2100 UTC 24 May of canopy resistance (s m^{-1}) for (a) CONTROL and (b) GEM.

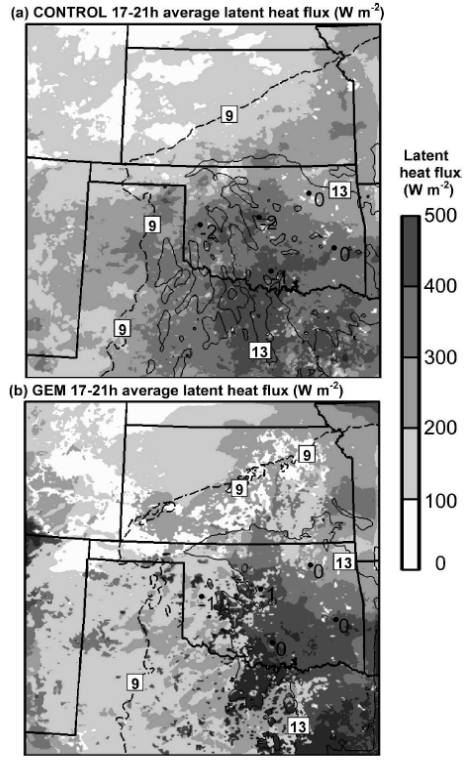

FIG. 15. Averaged 17–21-h latent heat flux (W m^{-2}) for (a) CONTROL and (b) GEM. The contours are for 9 (dashed) and 13 g kg^{-1} (solid) 2-m mixing ratio. Differences (model − obs) of mixing ratio for five selected mesonet stations are shown (solid circles) to illustrate the impact of latent heat flux differences.

Changes in surface fluxes after calibration:

Coupled simulated latent heat flux after off-line calibration reduces by 20 w/m2 respect to default parameter values run

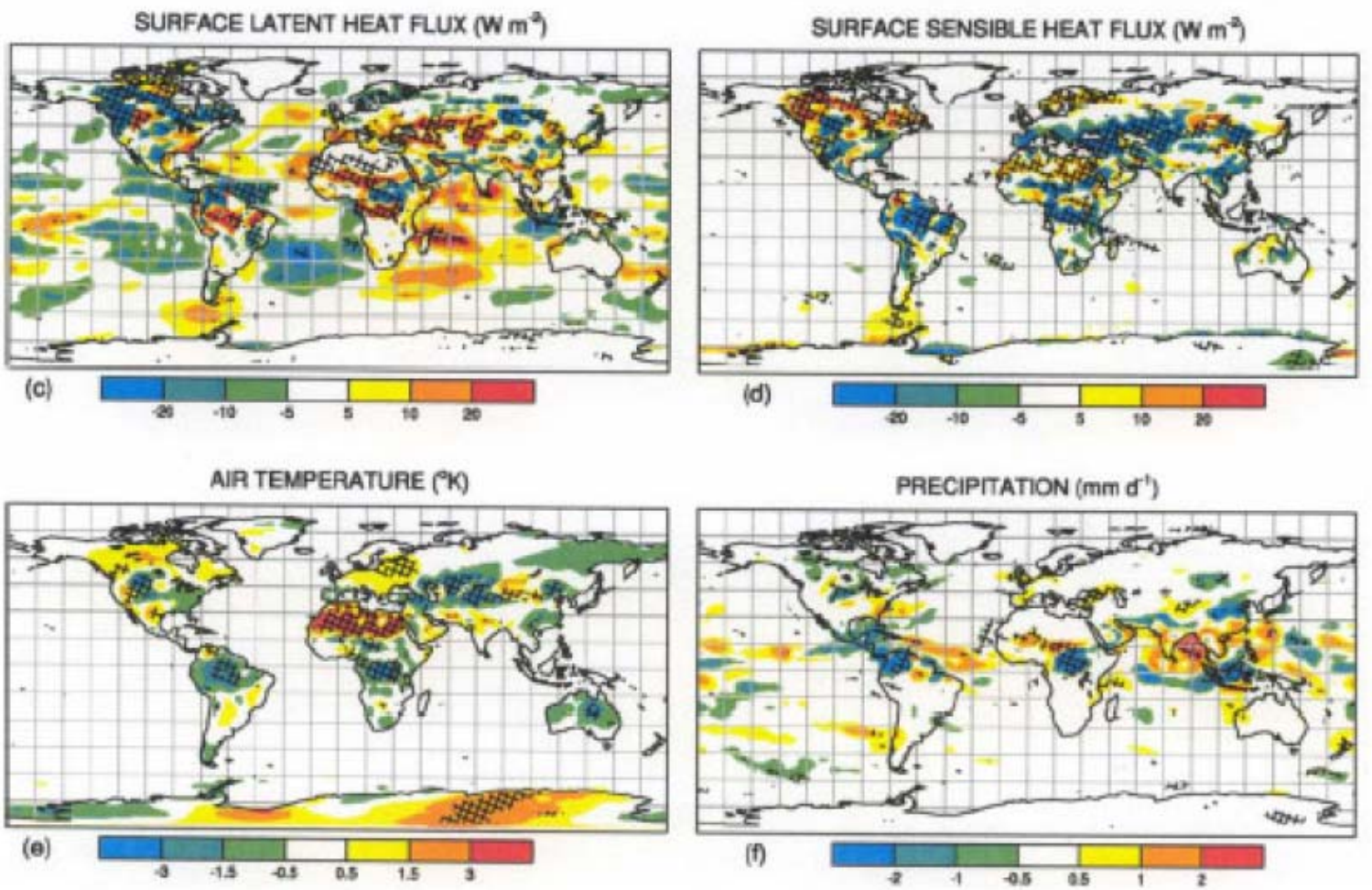

Fig. 8. *Eight-year average values for June, July, and August of differences in modelled (a) net solar flux, (b) net radiation, (c) latent-heat flux, (d) sensible heat flux, (e) air temperature, and (f) precipitation between simulations using BATS2 with parameters recalibrated using field data for the tropical forest, boreal forest, semi-desert, mixed crops and farming, and short grass biomes relative to susing default parameters. The hatched areas indicate where these differences are significant at the 95% confidence level [Taken from Sen* et al. *(2001)].*

Land memory: the role of soil moisture

Noah -HRLDAS increases the resolution of the assimilation system from 12 to 4 km.

Overestimates point measured LE, larger soil moisture amplitude , better captures spatial patterns.

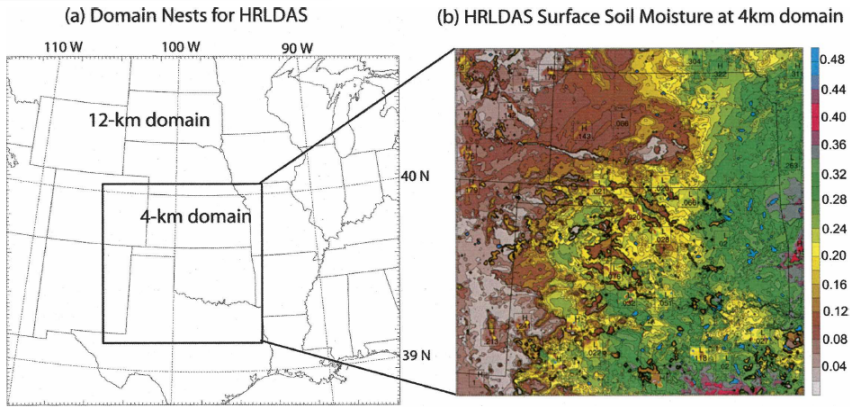

FIG. 1. Nested grids used for the HRLDAS IHOP_2002 experiment: (a) 12-km outer grid and 4-km inner grid and (b) HRLDAS surface volumetric soil moisture (contours in 0.02 m^3 m^{-3} intervals starting from 0.02 m^3 m^{-3}) valid at 1200 UTC 29 May 2002.

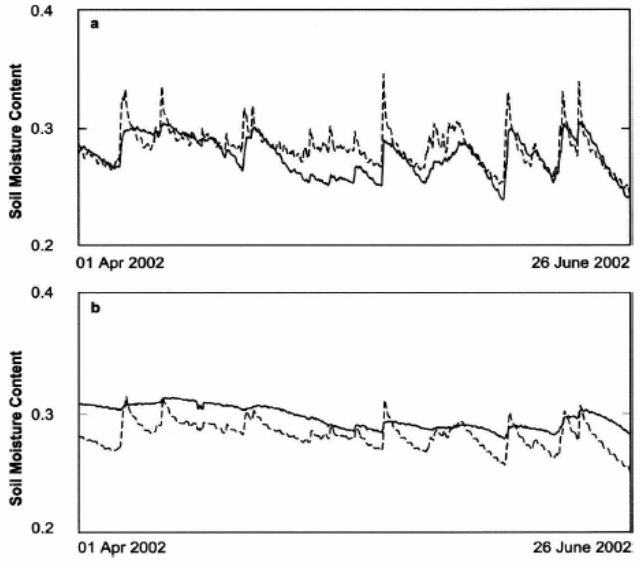

FIG. 10. Comparison of hourly volumetric soil moisture between HRLDAS and the Oklahoma Mesonet data, averaged over 30–65 mesonet stations: soil moisture at (a) 5 and (b) 25 cm for observations (solid line) and HRLDAS (dashed line).

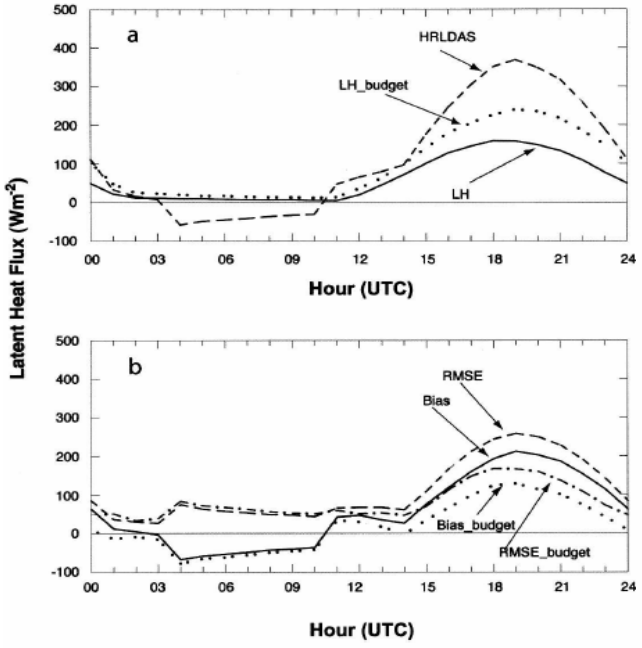

FIG. 9. As in Fig. 8, but for surface latent heat fluxes (W m^{-2}). (a) IHOP_2002 data (solid line), budget-derived IHOP_2002 latent heat flux (dotted line), and HRLDAS (dashed line); (b) bias computed using IHOP_2002 data (solid line), bias computed with budget-derived IHOP_2002 data (dotted line), RMSE computed with IHOP_2002 data (dashed line), and RMSE computed with budget IHOP_2002 data (dash–dot line).

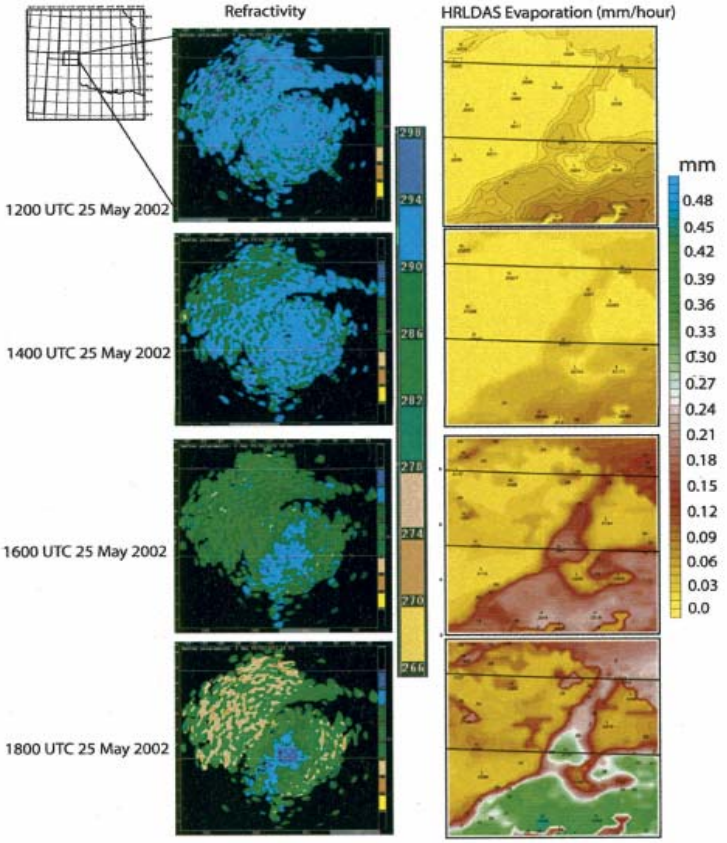

FIG. 12. Comparison between HRLDAS hourly surface evaporation (mm) and low-level water vapor (refractivity, N) derived fr NCAR S-Pol radar, valid at 1200, 1400, 1600, and 1800 UTC 25 May 2002. A change of 4N is approximately equivalent to a 1 g k change in water vapor. Blue and green shades represent regions of higher moisture.

Chen et al. 2007

Inverse modeling of van Genuchten soil parameters:

Noah runs with optimal parameters for both, Clap and Hornberger and van Genuchten provide nearly identical results. Latent heat flux RMSE is reduced by up to 60 W/m2 at all sites.

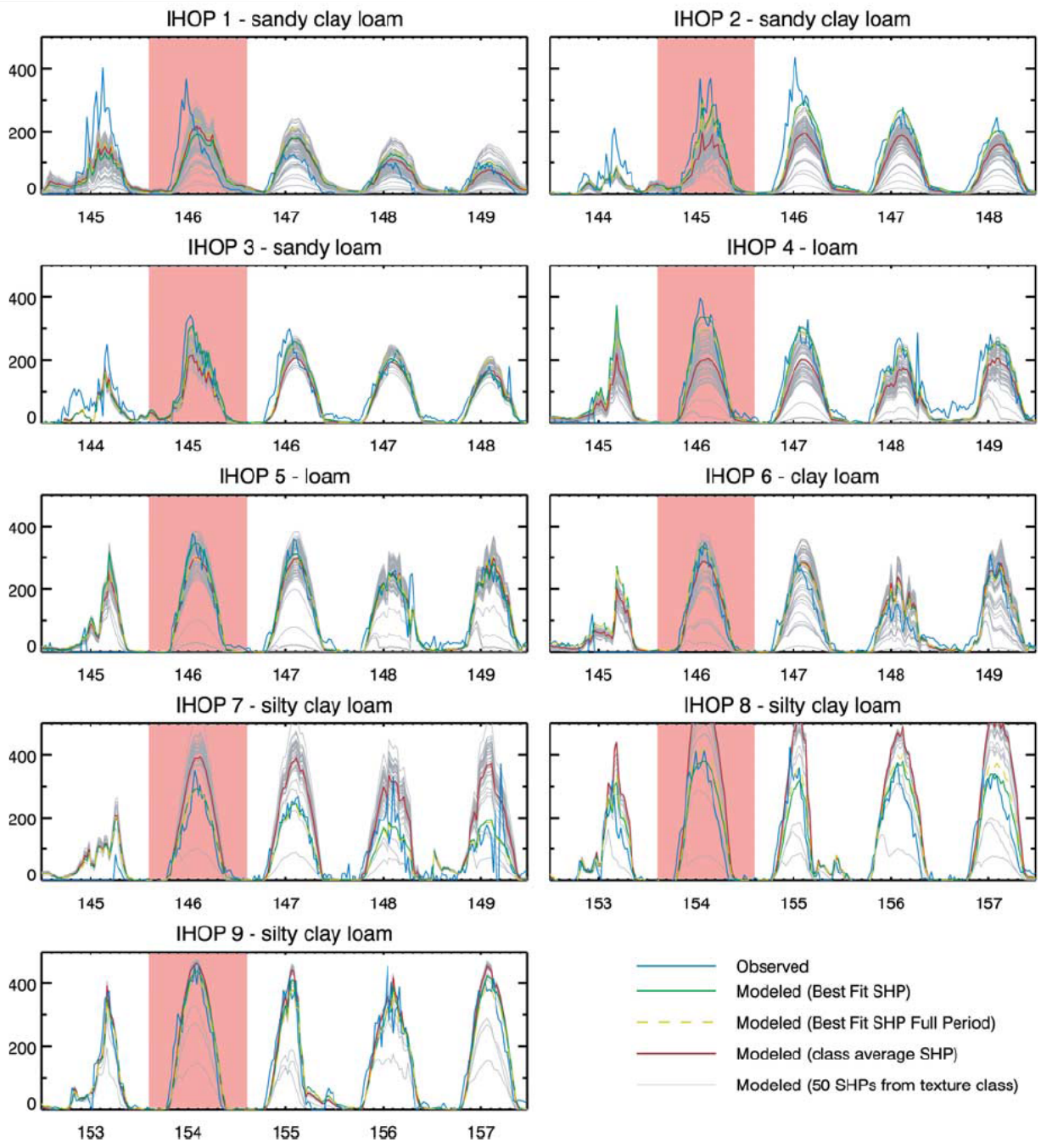

Figure 3. Time series of latent heat flux following a rainstorm at each site. Statistics for Tables 2a and 2b come from the day with shaded background. The X axis is the day of the year. A random subset of 50 soil hydraulic properties (SHPs) (dotted line) is presented at each site because if all soils are shown, it becomes impossible to distinguish individual lines. Individual SHPs (gray dotted line) come from the real soil texture class at each site. Measured LH (blue line), best fit SHP LH (green line), best fit SHP for the entire period LH (yellow dashed line), and texture class average SHP LH (red line) are also shown.

Gutmann and Small 2007

Enhancements to Noah physics:

Dynamic Vegetation after Dickinson et al., 1998

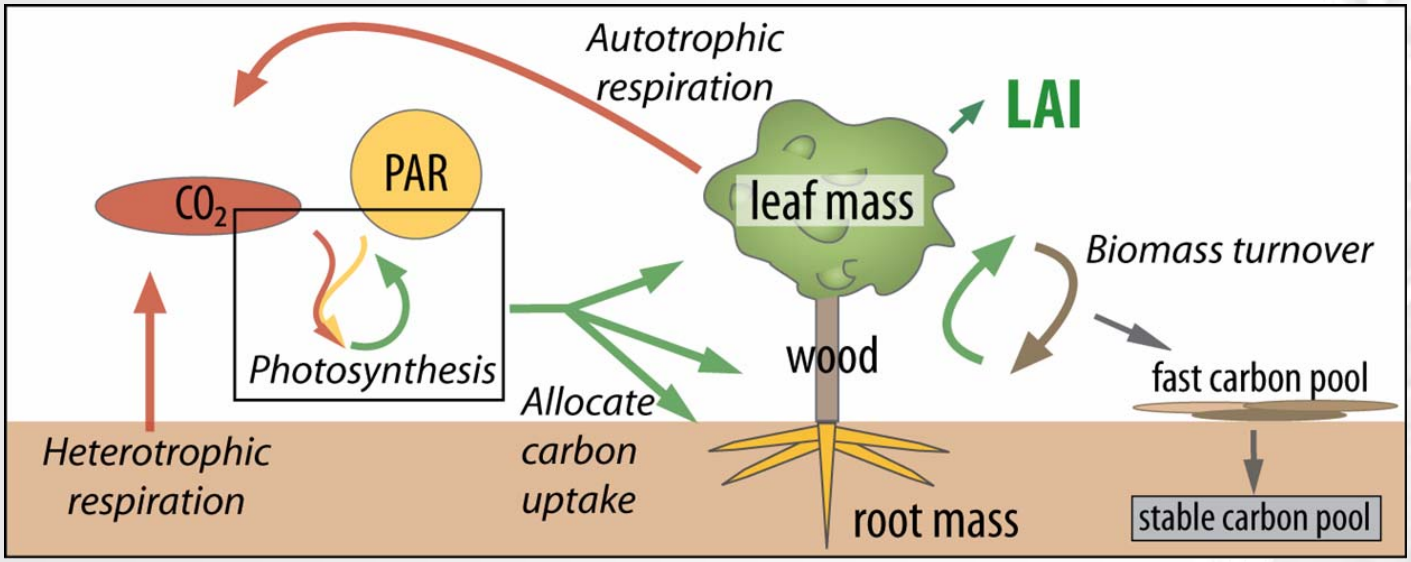

Groundwater after Niu et al., 2005, 2007.

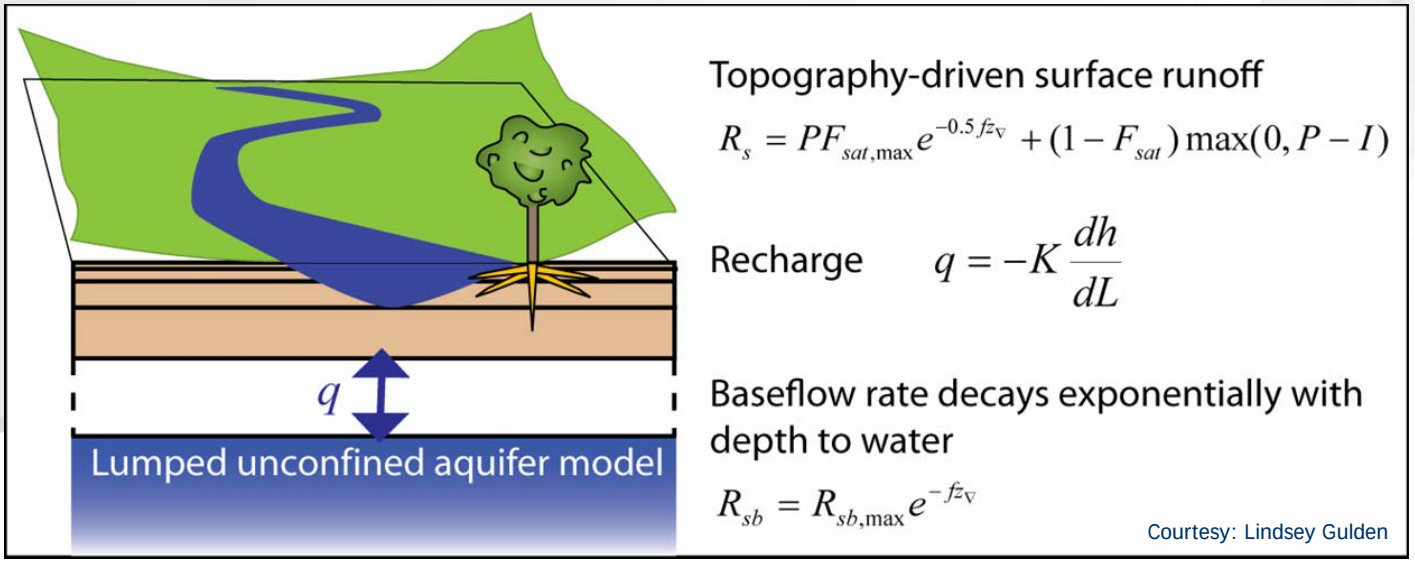

Courtesy: Lindsey Gulden

Experiment setup:

Hypothesis: increasing realism yields a model less sensitive to choice of parameters

Successive estimation of parameters for 4 models:

- ■ **Noah-STANDARD** (20 parameters: 10 soil, 10 vegetation) ▲ **Noah-DV** (+8 parameters, 28 total)
- ▼ **Noah-GW** (+4 parameters, 24 total)
- ★ **Noah-DVGW** (+12 parameters, 32 total)

Spin-up: NLDAS-forced run for ~2.5 years, no scoring.

Multi-objective, 5 constraints: Sensible heat (H), latent heat (LE), ground heat (G), first layer temperature STC(1) and first layer soil moisture SMC(1), scoring only 45 days.

Method: Markov Chain Monte Carlo sampler (MOSCEM, Vrugt et al., 2003). 250 par. sets approximate multivariate posterior distribution. 10,000 max number of function evaluations.

Calibration reduces only parameter uncertainty, exposes model error:

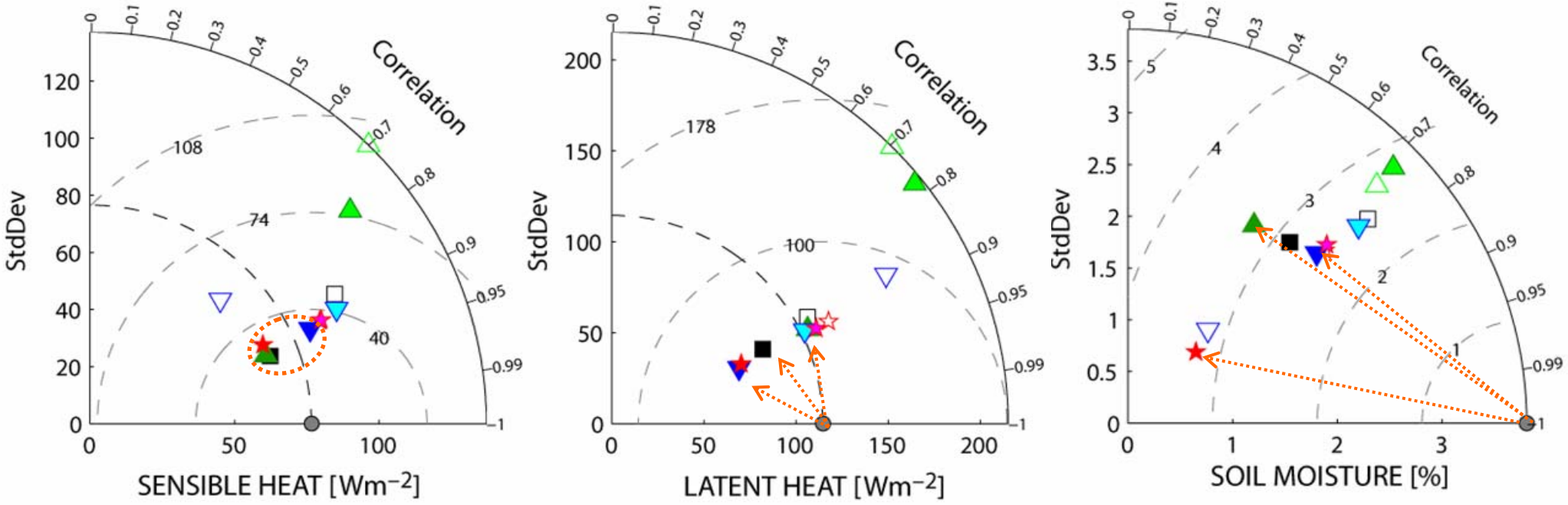

When parameter uncertainty is minimized, model performances are indistinguishable

THE UNIVERSITY OF TEXAS AT AUSTIN
JACKSON
SCHOOL OF GEOSCIENCES

At optimal state, model performances are indistinguishable; ‘working to characterize real contribution with other metrics

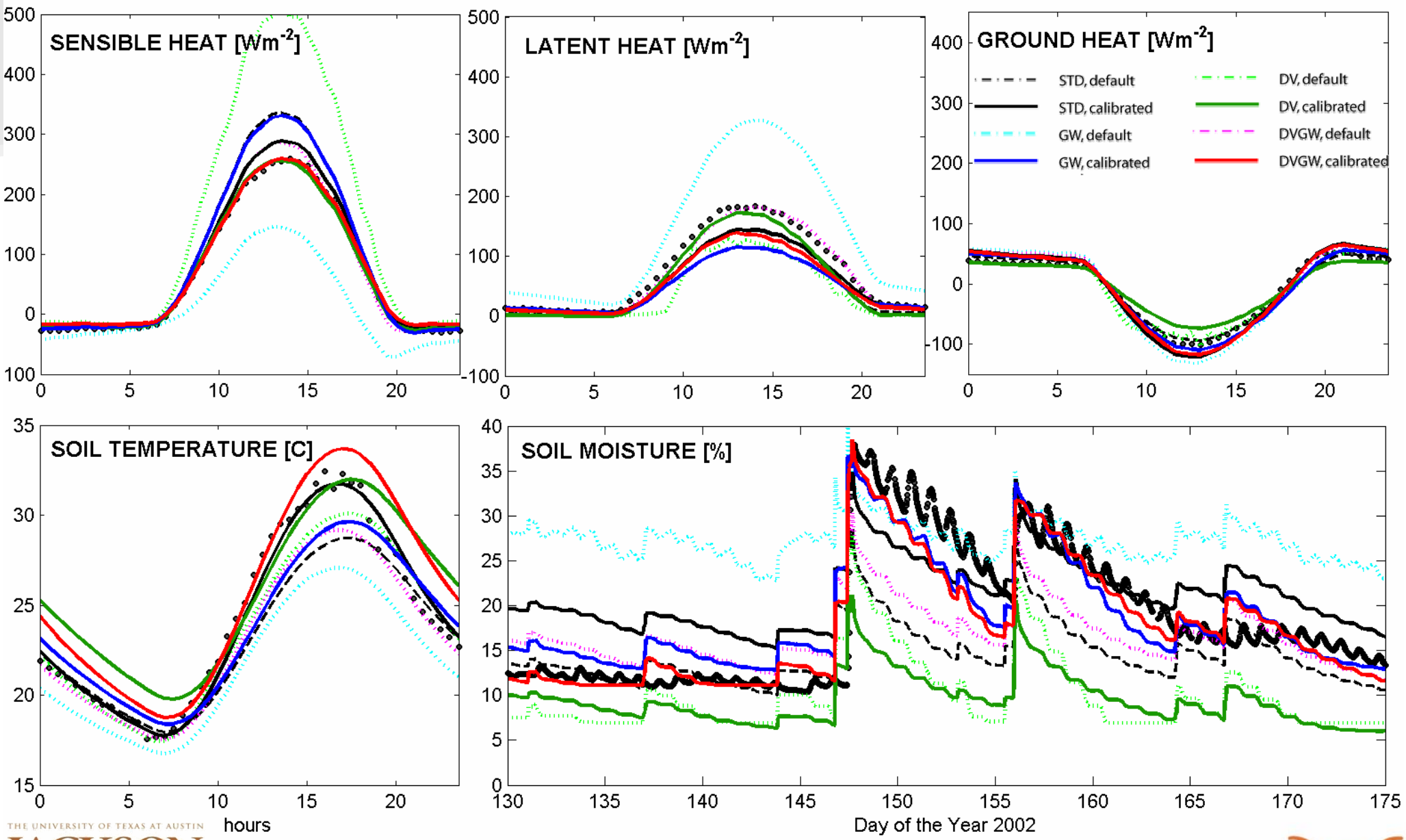

Summary and Conclusions

- Land-atmosphere coupling is strong in transition zones.
- Convection initiation by convergence is the main trigger for summertime precipitation in the Southern Great Plains.
- IHOP_2002 provides a wealth of data to evaluate land-surface parameterizations' ability to simulate fluxes that affect boundary layer processes.
- Noah LSM does a competent job of representing the diurnal cycle of surface fluxes and states.
- Photosynthesis-based evaporation schemes (dynamic phenology modules), subsurface hydrology (groundwater interaction) are in the forefront of LSM development.
- Calibration of effective parameters in complex models renders significant improvement.

Summary and Conclusions (cont.)

- Estimation of new model parameters only ("piecewise calibration") is often insufficient. (Only GW benefits from piecewise calibration.)
- When given optimum parameters **Noah-STD**, **Noah-DV**, **Noah-GW**, and **Noah-DVGW** perform equivalently well: model error remains the major component of the total uncertainty.
- Despite physical realism, parameters are still tunable coefficients: new default values needed.
- Added components alter host model structure; point of optimality shifts to accommodate new parameter interaction

Thanks!